Scientia Iranica F (2018) 25(3), 1824–1834

SCIENTIA IRANICA

Sharif University of Technology
Scientia Iranica
Transactions F: Nanotechnology
http://scientiairanica.sharif.edu

Realization of a reduced graphene oxide/ZnO nanorod photodetector, suitable for self-powered applications

L. Shafiei[a], S. Darbari[a,*], and F. Dehghan Nayeri[b]

a. *Department of Electrical and Computer Engineering, Tarbiat Modares University, Jalal Ale Ahmad Ave., Tehran, Iran.*
b. *Department of Electrical and Computer Engineering, University of Tehran, North Kargar Str., Tehran, Iran.*

Received 21 December 2016; received in revised form 16 August 2017; accepted 20 January 2018

KEYWORDS
ZnO nanorods;
Reduced graphene oxide;
Photodetector;
Nanogenerator;
Self-powered device.

Abstract. In this report, a reduced graphene oxide (rGO)/ZnO nanorod hybrid structure was proposed, benefiting from high photosensitivity and piezoelectric properties of ZnO nanorods, besides excellent carrier mobility, high optical transparency, and mechanical flexibility of the reduced graphene oxide sheets. Compared with the pristine ZnO nanorod-based structure, it was shown that the proposed hybrid photodetector exhibited improved output sensitivity to UV-illumination ($\Delta I/I = 424$). In addition, by taking advantage of the coupled semiconducting/piezoelectric properties of ZnO nanorods, the application of the proposed hybrid rGO/ZnO nanorod structure as a photosensitive piezoelectric nanogenerator was demonstrated. In this regard, enhanced open circuit voltage (1.5 V) and open circuit sensitivity ($\Delta V_{oc}/V_{oc} = -0.66\%$), besides a faster photoresponse, were achieved for the realized rGO/ZnO hybrid structure in comparison with ZnO nanorod-based counterpart. The observed enhancements were attributed to the presence of underlying reduced graphene oxide sheet as an efficient carrier transport layer in the proposed hybrid structure.

1. Introduction

Graphene is a 2-dimentional material with superior electrical and mechanical properties, including high electrical conductivity, chemical stability, significant transparency, and mechanical flexibility [1-3]. These attractive properties make graphene an excellent carrier transporter material in optoelectronic devices, benefiting from both high carrier mobility and optical transparency [4-6]. In this regard, some groups have applied semiconductor-graphene hybrid photodetectors and reported improved performances [7-9]. On the other hand, reduced Graphene Oxide (rGO) can be achieved by simple and low cost synthesis methods, showing properties similar to graphene sheets. Hence, there are numerous works which have utilized rGO sheets, benefiting from graphene-like properties [10,11].

ZnO is another attractive material that is a wide band-gap direct semiconductor, benefiting from low cost and environmentally friendly manufacturing, all of which entitle ZnO as an attractive candidate for photodetection applications. Among other nanostructures, 1-dimensional ZnO nanostructures have been widely used as building blocks in optoelectronic devices, owing to a one-dimensional carrier transport without scattering effect and high surface-to-volume ratio [12-14]. Owing to the piezoelectric property of ZnO nanorod, ZnO-based nanogenerators were proposed in 2006 to convert the environmental mechanical energy into electric energy [15-18]. Moreover, the coupling of piezoelectric and semiconducting properties in a material, like ZnO,

*. *Corresponding author. Tel. +98 21 82883524; Fax: +98 21 82884325*
E-mail addresses: lida.shafiei@modares.ac.ir (L. Shafiei); s.darbari@modares.ac.ir (S. Darbari); f.d.nayeri@gmail.com (F. Dehghan Nayeri).

doi: 10.24200/sci.2018.20149

led to an emerging field, known as piezophototronic, wherein strain-induced piezopotential was employed to tune the transport behavior of charge carriers in optoelectronic devices [19,20]. In this line of research, self-powered photodetectors were also proposed when scientists suggested that photogenerated carriers could modulate the piezopotential [7,21-23].

Considering the promising properties of rGO and ZnO, recently, there have been numerous reports that demonstrate the attractive behavior of rGO/ZnO hybrid structures in different application fields [24-29]. This report presents the fabrication of reduced graphene oxide (rGO)/ZnO nanorod hybrid structure and demonstrates the enhanced performance, both as a Metal-Semiconductor-Metal (MSM) photodetector and a self-powered photodetector. The rGO sheets have been synthesized by Hummer's method, and vertically aligned ZnO nanorods have grown on the dispersed rGO sheets by hydrothermal process subsequently.

2. Material and methods

Figure 1 displays the fabrication process schematically. As the first step of fabrication process, Au layer (100 nm) is deposited on a pre-cleaned soda lime glass by sputtering. Then, the metallic layer is patterned to interdigital electrodes with a spacing of about 10 μm (Figure 1(a)), serving as the electric contact of the proposed photodetector. In the next stage, Graphene Oxide (GO) sheets are achieved by the chemical exfoliation of graphite powder, according to the Hummers' method [30]. Now, the synthesized

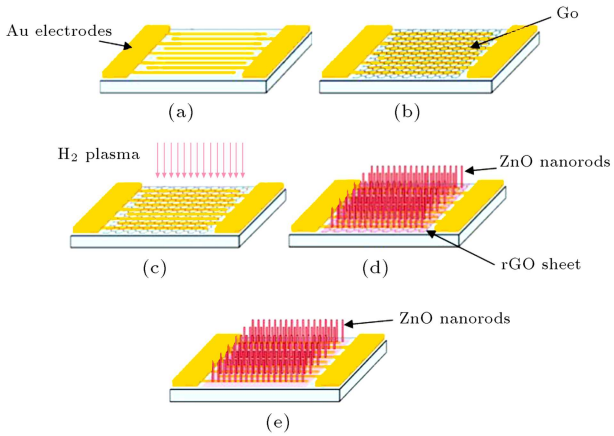

Figure 1. Fabrication process of the proposed rGO/ZnO nanorod-based photodetector: (a) Deposition and patterning Au layer on glass substrate, into interdigital electrodes, (b) dispersing GO sheets on the metallic electrodes, (c) hydrogenation-assisted reduction of the dispersed GO sheets, (d) growth of ZnO nanorods on the prepared sample to achieve rGO/ZnO nanorod-based photodetector, and (e) growth of ZnO nanorods directly on the pre-patterned metallic electrodes to achieve ZnO nanorod-based photodetector.

GO sheets are dispersed on the prepared sample by dip coating (Figure 1(b)). To reduce the dispersed GO sheets, the sample is placed in a plasma-enhanced chemical vapor deposition system and is exposed to hydrogen plasma with the power density of about 1 W/cm^2 for about 7 min (Figure 1(c)). This plasma-assisted reduction of GO sheets is carried out at a temperature of about 80°C, which allows for applying glass or flexible substrates. The hydrogen gas-in flow rate is about 20 sccm, while the base pressure is about 2 Torr in the course of this step.

To complete the structure of the proposed photodetector, ZnO nanorods should grow on the prepared sample, as depicted in (Figure 1(d)). A vertically aligned array of ZnO nanorods is utilized in order to benefit from the high surface area, one-dimensional transport of photogenerated carriers and high optical absorption in ZnO nanorod arrays. This enhanced absorption is expected from the enhanced light scattering in nanorod arrays, when sizes become comparable to incident wavelength. This enhanced light scattering can lead to optical birefringence [31] or optical funneling [32,33]. That is why arrays of nanorods, surrounded by air, can be utilized as stepped-index anti-reflection coatings [32,34]. On the other hand, inherently efficient induction of piezopotential in ZnO nanorods [21-23] will be applied to realize self-powered photodetectors (Section 3.3).

To achieve a vertically aligned nanorod array, first, a ZnO seed layer should be deposited on the sample [35]. It is notable that a successful growth of ZnO nanorods on rGO sheets by hydrothermal method has been previously demonstrated by taking advantage of a ZnO seed layer [36]. To prepare the seed layer, the sample is immersed in a solution of zinc acetate dehydrate in ethanol with concentration of 0.005 M and, then, is rinsed by ethanol and annealed at a temperature of 90°C. This procedure is repeated for about three times to achieve a 100 nm thick ZnO layer as the seed layer. After annealing the sample at 350°C for about 2 hours, the seed layer is crystallized and ready for the next step of hydrothermal growth [37]. The sample is placed in the chemical bath to synthesize ZnO nanorods [38]. For this purpose, a 100 ml aqueous solution of zinc nitrate ($Zn(NO_3)_2$-$6H_2O$, 99%) and hexamethylenetetramine (HMT) ($C_6H_{12}N_4$, 99%) are used as the growth chemical bath. In this growth solution, 20 mM levels of both $Zn(NO_3)_2$-$6H_2O$, and HMT are utilized. The solution is then placed in a capped Pyrex vessel, while the sample is exposed to the growth solution during stirring at a temperature of about 90°C. The synthesized nanostructures are ready after about 3 hours, washed, and, then, air-dried.

Figure 1(e) displays a ZnO-nanorod-based structure schematically fabricated with the similar process flow, excluding steps (b) and (c) in this figure. The

output behaviors of rGO/ZnO- and ZnO-based structures are compared to study the effect of underlying rGO layer on the detector's performance.

3. Result and discussion

3.1. Characterization

Figure 2(a) illustrates the result of the optical microscopy of the prepared interdigital electrodes on a glass substrate. The realized spacing between counter electrodes is about 10 μm in this structure. Part (b), in this figure, indicates the SEM image of the grown ZnO nanorods between the metallic electrodes. The inset shows a magnified view of the nanorods with an average diameter of about 100 nm. Figure 2(c) confirms an average length of about 1 μm for the grown nanorods. Notably, a few layers of rGO sheets are applied with a thickness of about 1 nm as the underlying layer in the ZnO/rGO-based structure. This rGO layer has negligible thickness in comparison with the ZnO seed layer (100 nm) so that the growth of ZnO nanorods cannot be affected by the presence of underlying rGO layer. This is in accordance with our observations in SEM results. To evaluate the thickness of the applied rGO sheets, AFM images from the dispersed sheets on glass are prepared, presented in Figure 3(a). Figure 3(b) depicts the height profile along with the black line in this image, indicating a thickness of about 1 nm, and reveals a few layers of rGO sheets ($<$ 3 layers). Figure 3(c) presents the absorbance spectrum of the synthesized GO sheets (solid spectrum) superimposed on the spectrum related to the rGO sheets (dashed spectrum) after hydrogenation process. A red shift can be observed in the absorbance spectrum of the rGO sample, compared with the GO specimen. Moreover, visible absorbance of rGO sheets is higher than that of GO sheets. These observations are attributed to the separation of oxygen groups and partial restoring of sp^2 carbon domains in the rGO sample as a result of a hydrogenation step [39].

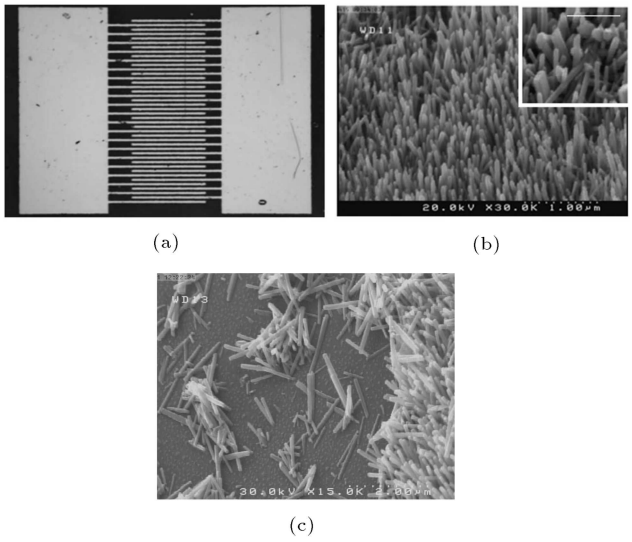

(a) (b) (c)

Figure 2. (a) Optical image of the prepared metallic electrodes, with interspacing of about 10 μm. (b) SEM image of the grown ZnO nanorods, between the interdigital electrodes. The inset shows the magnified view of the nanorods, with the scale bar of about 500 nm. (c) Cross section view of the grown ZnO nanorods.

Figure 3(d) presents the UV-vis spectrum of the grown nanorods by solid curve, which exhibits a sharp absorption edge rise at around 400 nm, coinciding with previous reports [36,40]. This figure also displays the optical absorbance of ZnO/rGO heterostructure (dashed spectrum), in which the absorbance edge of ZnO nanorods is detectable; however, the optical absorbance has been significantly increased due to the presence of rGO sheets [41]. To better investigate the structure of the prepared heterostructure, XRD analysis has been utilized, as depicted in Figure 3(e). Diffraction peaks and the indices, related to ZnO nanorods, are highlighted by solid arrows at 31.8°, 34.6°, 36.4°, 47.8°, and 63.2° [36,42]. It is observable that the relative intensity of the (002) reflection of ZnO surpasses others, indicating the dominant orientation of nanorods along the C-axis. Considering the low thickness of the underlying rGO layer in the prepared heterostructure, the trace of rGO is negligible in comparison with that of sharp ZnO peaks. However, a small hill-like peak is detectable at around 25°, attributed to the rGO sheet, which is in accordance with the literature data [36,42].

Figure 3(f) illustrates the Raman spectrum of the synthesized graphene oxide sheets before (red spectrum) and after (black-dashed spectrum) reduction, which clearly shows the typical characteristics of carbon materials. The observed spectrum exhibits three individual peaks called D and G bands, which are around 1305 cm^{-1}, 1572 cm^{-1}, respectively. G band corresponds to sp^2 carbon-type structures within the sheets, while D band is assigned to the structural imperfections in the hexagonal graphitic layers induced by the attachment of hydroxyl or epoxide groups. Concerning this, higher D peak intensity in a Raman spectrum can be assigned to higher defects and disorders of the graphitized structures, higher fraction of sp^3/sp^2-bonded carbon, and/or smaller size of the in-plane graphitic crystallite sp^2 domains. Based on this figure, I_D/I_G value decreases significantly after reduction process, which is related to the reduction of the graphene oxide sheets and development of sp^2 domains, as a consequence of hydrogenation process [43,44].

Next, the electrical characteristics of the realized samples have been investigated before and after reduction. Figure 4 indicates the I-V characteristic of the prepared sample after dispersing GO sheets on

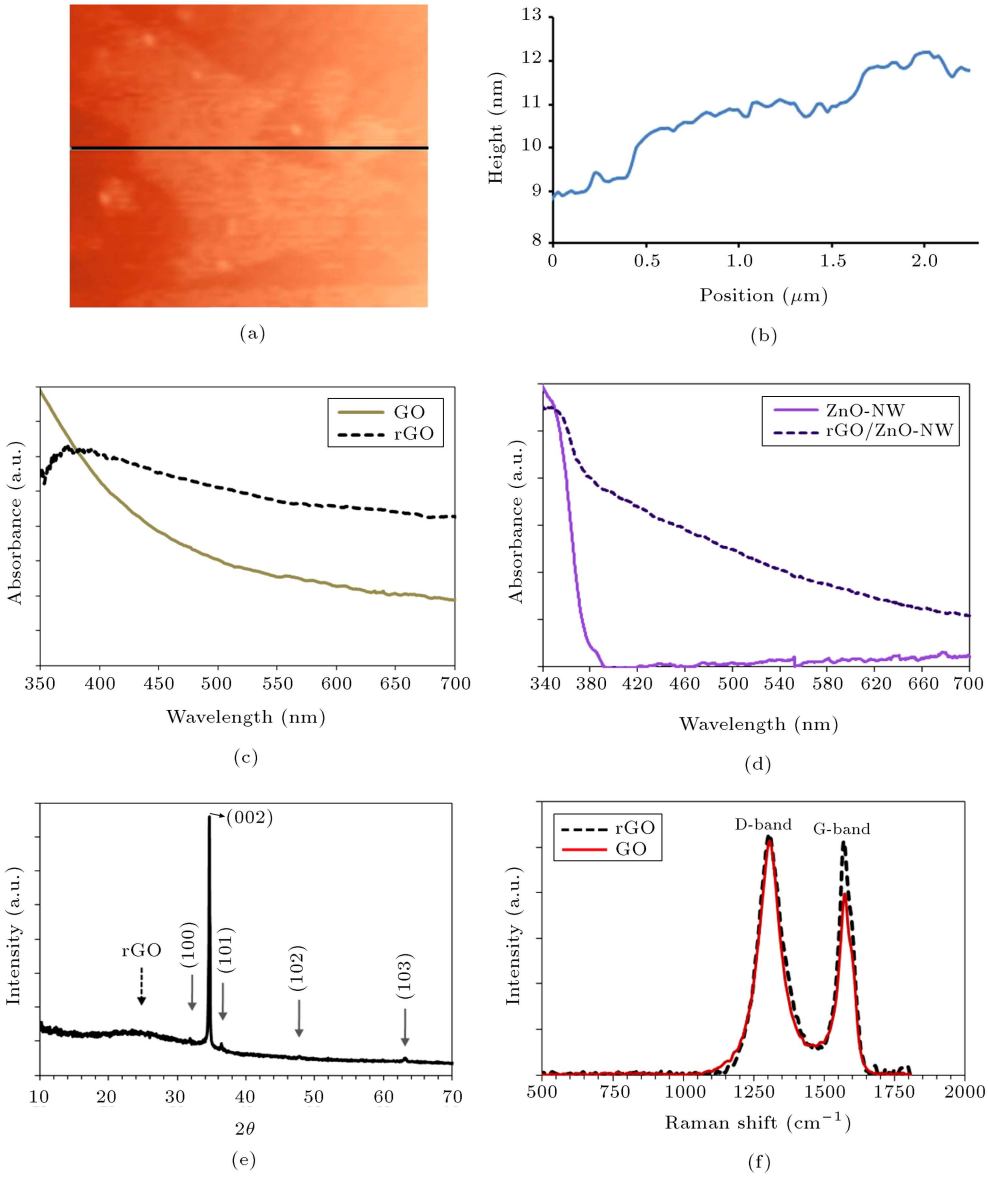

Figure 3. (a) and (b) AFM image and the corresponding height profile (along the black line) of the prepared rGO sheets on glass. (c) UV-vis spectrum of the synthesized GO sheets (solid spectrum) superimposed on the rGO sheets (dashed spectrum). (d) UV-vis spectra of the synthesized ZnO nanorods (solid spectrum), and the ZnO/rGO heterostructure (dashed spectrum). (e) XRD analysis of the synthesized ZnO/rGO heterostructure. (f) Raman spectra of the synthesized GO sheets, before (red spectrum) and after (black-dashed spectrum) reduction process.

interdigital Au electrodes (yellow curve), according to Figure 1(c). The schematic in the inset manifests the electrical measurement in this step. The measured current is negligible before reduction, which is magnified in the inset of this figure. After hydrogenation (blue curve), an improvement of approximately 100 times can be observed in the electrical conductivity, attributed to removing hydroxyl groups and restoring π-network in the rGO sheet. The other worthy point is that electrical behavior of Au/GO/Au structure (inset) converts into nearly a linear behavior in Au/rGO/Au structure, which is in accordance with restoring semimetallic characteristics in rGO sheets after reduction.

3.2. Output behavior of rGO/ZnO-based MSM photodetector

To investigate the output response of the fabricated rGO/ZnO photodetector, first, I-V characteristics of the device have been investigated when exposed to illumination. Laser sources with equal output power and different wavelengths of about 380 nm, 560 nm, and 660 nm have been utilized in this experiment. In addition, notably, to highlight the effect of the underlying rGO layer on the output performance of the realized photodetector, a similar device based on ZnO nanorods (Figure 1(e)) has been prepared, and the corresponding output behavior has been compared with the proposed

rGO/ZnO structure. Figure 5(a) and (b) demonstrate I-V characteristics of the prepared ZnO and rGO/ZnO structures on a logarithmic scale, in dark conditions (black curve), and when exposed to red (red curve), green (green curve), and UV (violet) illuminations. As expected, Figure 5(a) illustrates that ZnO-based structure does not show any detectable photoresponse to red illumination, however a slight photoresponse is detectable for green illumination and a considerable response is measured as a result of UV illumination. The observed significant photoresponse of the ZnO-based detector is in agreement with the wide band gap of ZnO nanostructures. In addition, the measured photoresponse to green illumination is attributed to the structural defects and surface dangling bonds present in the synthesized ZnO nanorods, which can lead to local energy states inside the forbidden band gap [45].

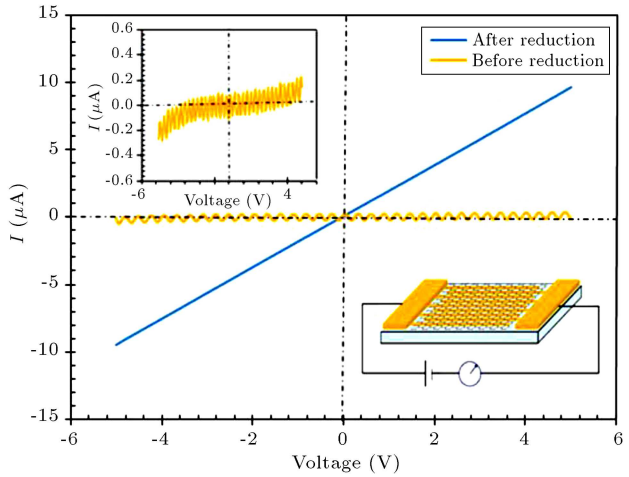

Figure 4. I-V characteristics of the GO (yellow curve) and rGO sheets (blue curve), dispersed between the interdigital electrodes. The left-top inset magnifies the electric characteristic of the GO sheet, before reduction. The bottom-right inset manifests the structure under test, schematically.

Based on Figure 5(b) the measured dark current of the rGO/ZnO structure has increased about 10 times in comparison with the ZnO structure. This conductivity enhancement is attributed to the presence of underlying rGO layer. Parts (c-e), in this figure, show the time-resolved photoresponse of the fabricated photodetector based on rGO/ZnO structure, to UV, green, and red illuminations, respectively. The bias voltages are about 1 V in these experiments. Table 1 shows output sensitivity ($S = (I_{\text{light}} - I_{\text{dark}})/I_{\text{dark}}$) of the fabricated structures in response to different

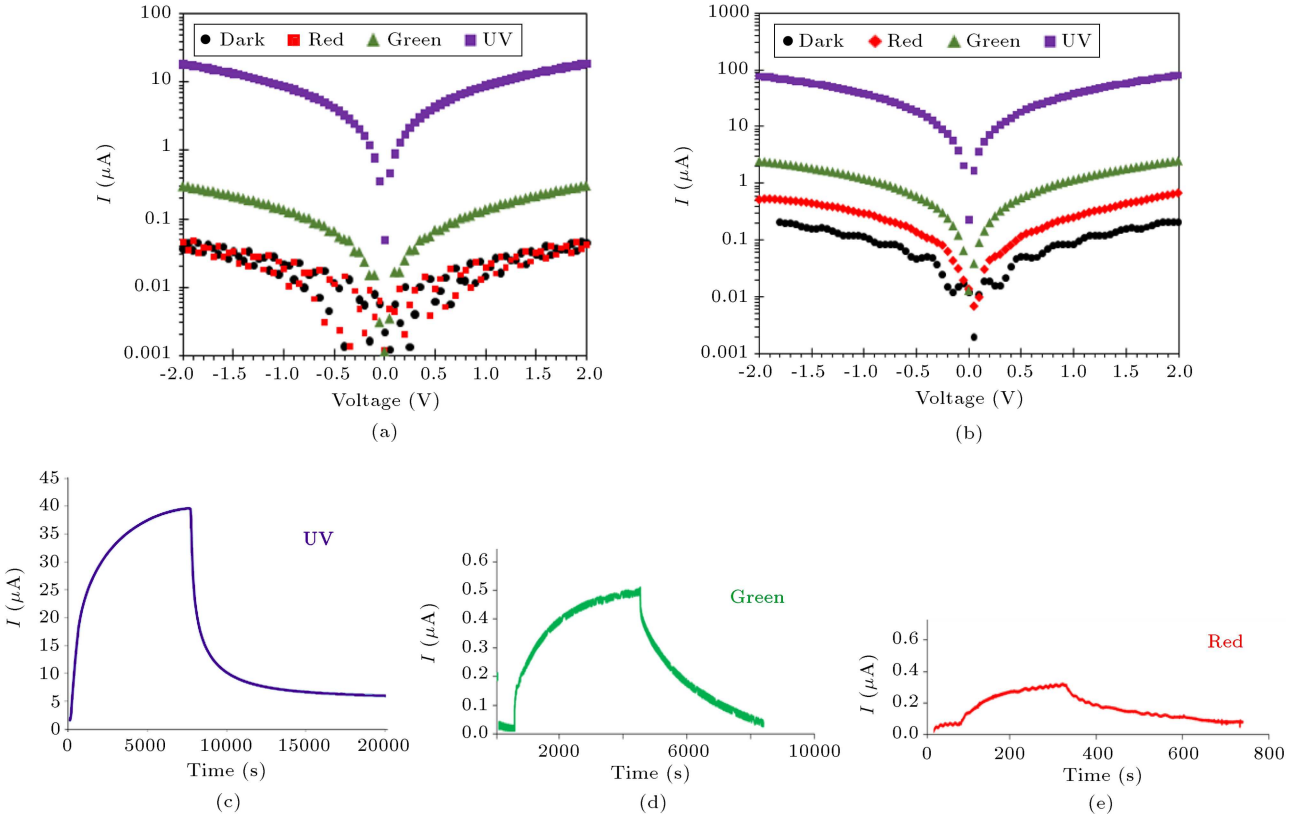

Figure 5. Optoelectric characteristics of the fabricated photodetectors, when exposed to dark condition (black curve) and UV (violet curve), green (green curve), red (red curve) illuminations: (a) ZnO nanorod-based photodetector, (b) rGO/ZnO nanorod-based photodetector, and (c-e) time resolved response of the fabricated ZnO/rGO-based photodetector to UV, green and red illuminations.

Table 1. Output sensitivities of the realized rGO/ZnO and ZnO structures in response to different incident wavelengths.

		Sensitivity		
		UV	**Green**	**Red**
Structure	**ZnO**	399	6.5	0
	rGO/ZnO	424	11.3	1.6

illumination wavelengths. It is shown that rGO/ZnO structure shows better sensitivity in all illumination wavelengths, attributed to lower transit time of the photogenerated carriers through rGO sheet. The other point observed in this table is that there is not any measurable output sensitivity to red illumination in the ZnO structure; however, the rGO/ZnO structure shows detectable sensitivity. This observation can be related to both the photogenerated carriers in rGO and the trap-assisted photogenerated carriers in ZnO, which are originated from the carbon-induced midgap subbands [8]. Moreover, it is notable that the reported output Sensitivity (S) is enhanced by about two orders of magnitude, compared to previously reported photodetector based on rGO/ZnO nanoparticle [8] at similar bias voltages. The observed synergic effect of rGO and ZnO nanorods on the realized hybrid UV photodetector can be attributed to the high optical absorption in the ZnO nanorod array, effective charge transfer between the ZnO/rGO interface, and fast-charge transport by rGO.

Figure 6 demonstrates the structure of the realized rGO/ZnO photodetector (Figure 6(a)) and the operation mechanism of the device (Figure 6(b)), when exposed to illumination. It is known that surface processes in optoelectronic devices based on ZnO nanostructures play a crucial role due to large surface-to-volume ratios [46-50]. It can be observed in

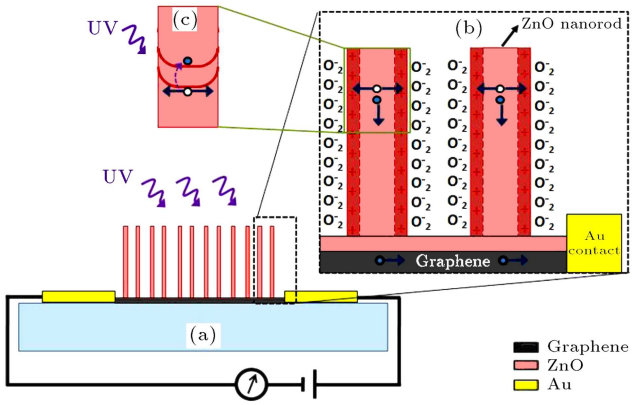

Figure 6. (a) The carriers transport model for the realized rGO/ZnO detector. (b) Detailed schematic which shows the surface oxygen absorption and formation of a depletion layer, consequently. (c) The corresponding energy band diagram of the nanorods, and separation of the photogenerated e/h pairs.

Figure 6(b) that, in dark conditions, oxygen molecules are adsorbed on the surface of ZnO nanorods; then, an electron is taken and a depletion layer is created consequently [$O_2(g) \leftrightarrow O_2(ad)$, $O_2(ad) + e \rightarrow O_2^-(ad)$]. Upon UV illumination, the surface-adsorbed oxygen molecules capture the photo-generated holes Figure 5(b), thus narrowing the depletion region in the ZnO nanorods [$O_2^-(ad) + h^+ \rightarrow O_2(g)$]. It should be noted that this surface-induced separation of photogenerated carriers prevents the recombination of photogenerated carriers and results in high output sensitivity in ZnO nanostructures. Figure 6(c), also, displays the band diagram of the ZnO nanorods with a band bending across the depletion layer. It is shown that the photogenerated holes are adsorbed onto the surface of nanorods, and they interact with negative oxygen ions. On the other hand, electrons can transport toward the underlying graphene layer and, then, transit the metallic electrodes. High mobility of carriers in graphene leads to an increment in the output sensitivity in rGO/ZnO structure, compared with the ZnO-based device.

To elaborate on the effect of structural parameters of ZnO nanorods on the photoresponse of the fabricated photodetector based on rGO/ZnO, the growth conditions have changed to achieve ZnO nanorods with different diameters. For this purpose, the molar ratio of $Zn(NO_3)_2 - 6H_2O$ to HMT as 0.5 (Sam1), 1 (Sam2), and 2 (Sam3). It is well known that the concentration of Zinc precursor affects the diameter of the ZnO nanorods [51]. Table 2 summarizes the achieved average rod diameter and the UV sensitivity of the related achieved samples. It is shown that the molar ration of $Zn(NO_3)_2$: HMT increases the rod diameter from about 70 nm to 280 nm; however, the observed UV-sensitivity is maximized for Sam2 with the rod diameter of about 100 nm.

3.3. Realization of rGO/ZnO-based self-powered photodetector

After demonstrating high efficiency of the realized rGO/ZnO photodetector in the previous part, a novel self-powered photodetector based on rGO/ZnO nanorods is proposed. Herein, the coupled semiconducting/piezoelectric properties of ZnO are utilized to convert mechanical energy into electricity. The concept

Table 2. Output sensitivities of rGO/ZnO-based photodetectors (Sam1, Sam2 and Sam3) to UV illumination.

	Sam1	**Sam2**	**Sam3**
$Zn(NO_3)_2$: HMT	0.5	1	2
Rod diameter (nm)	70	100	280
S_{UV} $(\Delta I/I)$	37.7	424	221.9

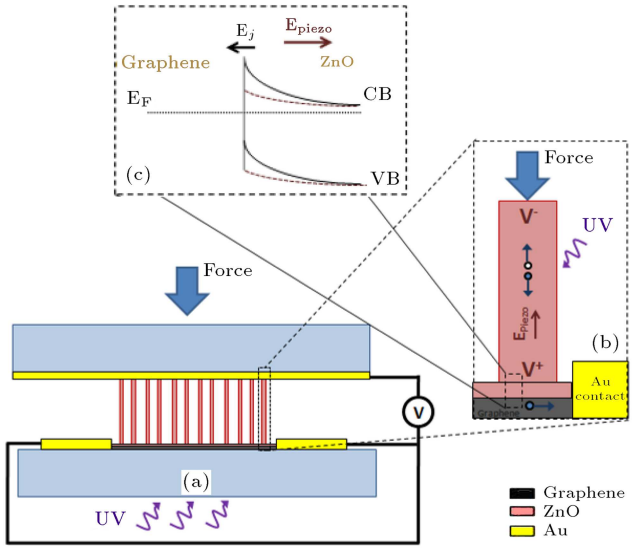

Figure 7. (a) Structure of the proposed self-powered photodetector, based on rGO/ZnO structure. (b) Operation principle of the proposed structure: External force induces a piezopotential along the ZnO nanorods and photogenerated carriers screen the induced piezopotential, when exposed to UV-illumination. (c) Band diagram of the rGO/ZnO junction which shows Schottky barrier lowering as a result of piezoelectric field.

of "self-powered devices" can supply power to electrical devices without the need for batteries. In the last few years, there are some reports which have utilized ZnO to realize self-powered photodetectors [21-22,49-50].

To elaborate on the behavior of the fabricated ZnO/rGO-based self-powered photodetector, an Au-coated glass on the ZnO nanorods has been placed, as depicted in Figure 7(a). It is known that piezoelectric nanogenerators generally consist of piezoelectric nanostructures, sandwiched between a bottom ohmic contact and a top Schottky contact, in order to effectively convert the external mechanical stress to electric current and prevent the compensating currents. In this structure, the bottom rGO/ZnO contact (with a weak Schottky barrier) can behave approximately as an ohmic contact [52], and the Au/ZnO contact plays a role as the Schottky contact due to a high-work-function Au electrode. In addition, it is notable that, in this experiment, the external pressure is applied to the upper Au electrode, and the incident light is illuminated on the backside of the sample (Figure 7(a)). Herein, both high optical transparency and high electric conductivity and mechanical flexibility of underlying rGO layer are utilized to enhance the output optoelectric behavior. As shown in Figure 7(a), interdigital electrodes are connected to each other in this experiment, and the output electric contacts are extracted from the up and bottom layers of Au. When an external force is applied to ZnO nanorods, a piezopotential is created internally so that negative potential can be induced on the compressed side of the nanorods (Figure 7(b)). Hence, an external mechanical force leads to an open circuit voltage, which can be measured between the up/bottom electrodes. When there is a simultaneous UV illumination, the photogenerated electron/hole pairs are drifted according to the piezoelectric field, which screen the force-induced piezoelectric voltage and lower the output open circuit voltage (Figure 7(b)). The other worthy point is Schottky barrier lowering as a consequence of the induced piezopotential at the ZnO/rGO contact. Figure 7(c) illustrates the band diagram of the realized ZnO/rGO interface with (solid bands) and without (dashed bands) force-induced piezoelectric field. It can be observed in this schematic that exerting force on ZnO nanorods results in lowering the small Schottky barrier at the bottom of ZnO/rGO interface and realization of nearly an ohmic contact. This effect can be beneficial for harvesting energy behavior of the structure efficiently.

Figure 8(a) and (b), show the optoelectric characteristics of the fabricated-ZnO and rGO/ZnO-based

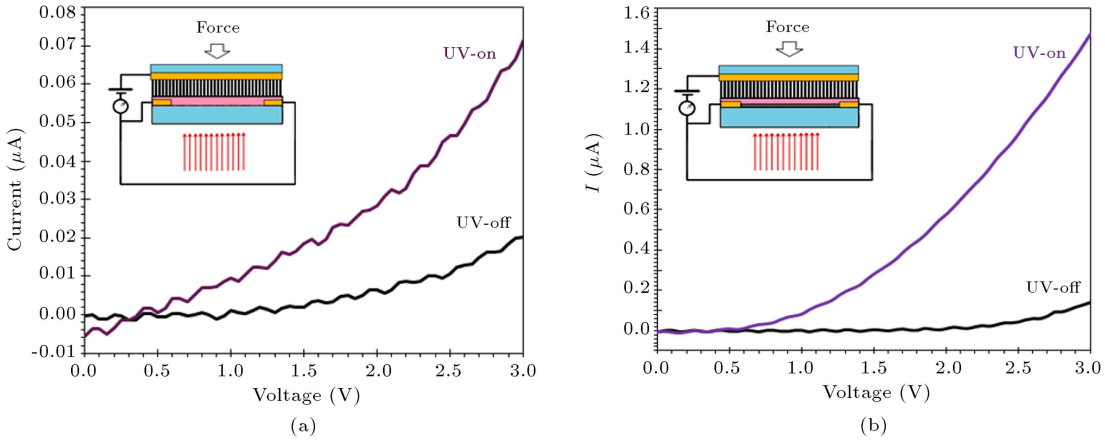

Figure 8. Optoelectric characteristics of the realized (a) ZnO-based, and (b) rGO/ZnO-based structures, while a constant force is exerted to the devices. Insets display the investigated structures and the test configuration, schematically.

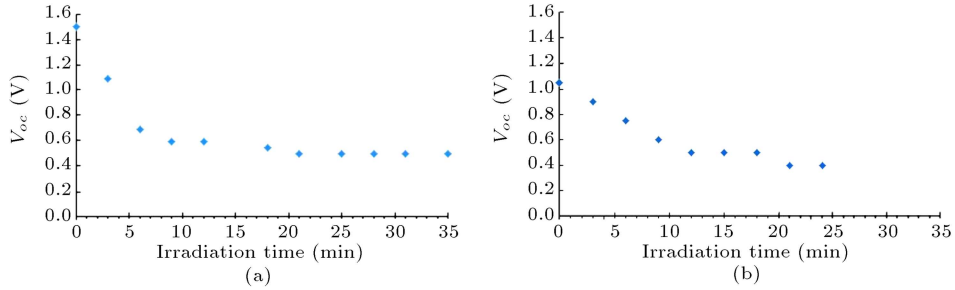

Figure 9. Time-resolved variation of the measured open circuit voltage of (a) rGO/ZnO-based, and (b) ZnO-based self-powered photodetectors.

structures. It is notable that a constant compressive force is exerted on the NG in this experiment. The insets display the corresponding investigated structures, schematically. It can be observed in this figure that the measured dark current is higher in rGO/ZnO structure than that in the ZnO-based structure, which is attributed to high conductivity of underlying rGO layer. In addition, the optoelectric sensitivity $\frac{I_{\text{light}}-I_{\text{dark}}}{I_{\text{dark}}}$ is higher in rGO/ZnO structure (∼14) for:

$$V_{\text{bias}} = 3V,$$

compared with ZnO structure (∼2.5). This observation can be also related to the superior electrical conductivity of rGO, in comparison with ZnO layer, so that the photogenerated electrons can transit and be collected by Au electrodes, efficiently and rapidly. It is notable that the internal piezoelectric field can play a crucial role in preventing the recombination of photogenerated carriers and increasing the optoelectric sensitivity. Similarly, the weak Schottky contact at the interface of ZnO/rGO layer can help separate photogenerated carriers near the junction and lead to the enhancement of the optoelectric sensitivity.

Figure 9 displays the measured open circuit voltage of the realized rGO/ZnO and ZnO structures, versus UV-irradiation time. It can be observed that, for both structures, open circuit voltage decreases by UV illumination which is related to the screening of piezopotential by photogenerated carriers. In addition, the measured open circuit voltage in a dark condition is higher for rGO/ZnO-based nanogenerator than that for ZnO-based nanogenerator. The observed open circuit sensitivity is measured to be about –66% and –61%, for rGO/ZnO and ZnO structures respectively. The achieved enhancements, both in the open circuit voltage and open circuit sensitivity ($S_{oc} = \Delta V_{oc}/V_{oc}$) of the proposed rGO/ZnO self-powered photodetector are believed to be the result of the lower series resistance, corresponding to the underlying rGO layer in comparison with ZnO. Different bottom Schottky barriers also can be responsible for the observed higher open circuit voltage. As shown in the insets of Figure 8, ZnO/rGO junction is a low Schottky barrier contact which is present at the bottom junction of ZnO/rGO-based sample, while ZnO/Au junction is present at the bottom junction of ZnO-based sample and forms a high Schottky barrier. As depicted in Figure 7(c) the junction-related electric field of the bottom Schottky contact opposes the force-induced piezoelectric field in nanorods. Hence, it is expected that the force-induced open circuit voltage is stronger for rGO/ZnO-based nanogenerator, which is in accordance with measurement results in Figure 9.

Table 3. Output characteristics of the realized rGO/ZnO and ZnO based self-powered photodetectors.

		V_{oc} (V)	S_{oc} (%)	t_{fall} (min)
Structure	**ZnO**	1.05	61	12
	rGO/ZnO	1.5	66	6

The other worthy point is the faster response of the realized rGO/ZnO self-powered detector in comparison with the ZnO structure. The measured fall time is about 6 min for rGO/ZnO-based self-powered photodetector, while a fall time of about 12 min is measured for ZnO structure. The lower transit time of carriers in rGO is believed to be the main reason for the observed improved transient response. In addition, it should be noted that the relatively slow photoresponse of both structures is attributed to the role of ZnO nanostructures, as the absorbing layer, and the previously discussed adsorption/desorption of oxygen molecules on the surface of nanorods [8].

Table 3 summarizes the achieved output characteristics of the realized self-powered photodetectors, highlighting the improved photoresponse of the rGO/ZnO-based nanogenerator in comparison with the ZnO-based structure.

4. Conclusion

This study proposed the rGO/ZnO hybrid photodetector and demonstrated the enhanced sensitivity of about 424 in response to UV illumination, as compared with bare ZnO structure. Then, it proposed the realized rGO/ZnO hybrid structure as a self-powered photodetector, in which ZnO nanorods array behaved as the

absorbing piezoelectric layer. Applying external force to the structure resulted in the creation of piezoelectric potential and the modification of the bottom rGO/ZnO Schottky barrier. Simultaneous photo-illumination generated electron/hole pairs which can screen the piezopotential and reduce the measured open circuit voltage. Our study showed an enhanced open circuit sensitivity (–66%), in addition to higher open circuit voltage (1.5 V), and also faster photoresponse for the proposed self-powered rGO/ZnO structure, compared with a similar ZnO-based structure. According to the achieved results, the proposed rGO/ZnO hybrid structure can be entitled as an attractive candidate for piezophototronic applications and can open up new horizons for self-powered devices.

Acknowledgments

The authors would like to acknowledge the partial financial support of the Iran National Science Foundation (INSF) 95821267.

References

1. Du, X., Skachko, I., Barker, A., and Andrei, E.Y. "Approaching ballistic transport in suspended graphene", *Nature Nanotech.*, **3**(8), pp. 491-495 (2008).
2. Geim, A.K. and Novoselov, K.S. "The rise of grapheme", *Nature Mater.*, **6**(3), pp. 183-191 (2007).
3. Song, J.C., Rudner, M.S., Marcus, C.M., and Levitov, L.S. "Hot carrier transport and photocurrent response in grapheme", *Nano Lett.*, **11**(11), pp. 4688-4692 (2011).
4. Nair, R.R., Blake, P., Grigorenko, A.N., Novoselov1, K.S., Booth, T.J., Stauber, T., Peres, N.M.R., and Geim, A.K. "Fine structure constant defines visual transparency of grapheme", *Sci.*, **320**(5881), pp. 1308-1308 (2008).
5. Neves, A.I.S., Bointon, T.H., Melo, L.V., Russo, S., de Schrijver, I., Craciun, M.F., and Alves, H. "Transparent conductive graphene textile fibers", *Sci. Rep.*, **5**(9866), (2015).
6. Zhang, X., Yan, X., Chen, J., and Zhao, J. "Large-size graphene microsheets as a protective layer for transparent conductive silver nanowire film heaters", *Carbon*, **69**, pp. 437-443 (2014).
7. Saravanakumar, B., Thiyagarajan, K., Alluri, N.R., Yoon, S.S., Taehyun, K., Lin, Z.H., and Kim, S.J. "Fabrication of an eco-friendly composite nanogenerator for self-powered photosensor applications", *Carbon*, **84**, pp. 56-65 (2015).
8. Zhan, Z., Zheng, L., Pan, Y., Sun, G., and Li, L. "Self-powered, visible-light photodetector based on thermally reduced graphene oxide-ZnO (rGO-ZnO) hybrid nanostructure", *J. Mater. Chem.*, **22**(6), pp. 2589-2595 (2012).
9. Liu, H., Sun, Q., Xing, J., Zheng, Z., Zhang, Z., Lü, Z., and Zhao, K. "Fast and enhanced broadband photoresponse of a ZnO nanowire array/reduced graphene oxide film hybrid photodetector from the visible to the near-infrared range", *ACS Appl. Mater. Interfaces*, **7**(12), pp. 6645-6651 (2015).
10. Singh, R.K., Kumar, R., and Singh, D.P. "Graphene oxide: strategies for synthesis, reduction and frontier applications", *RSC. Adv.*, **6**, p. 64993 (2016).
11. Kumar, R., Singh, R.K., Singh, D.P., Joanni, E., Yadav, R.M., and Moshkalev, S.A. "Laser-assisted synthesis, reduction and micro-patterning of graphene: Recent progress and applications", *Coordination Chem. Rev.*, **342**, pp. 34-79 (2017).
12. Zhang, Y., Ram, M.K., Stefanakos, E.K., and Goswami, D.Y. "Synthesis, characterization, and applications of ZnO nanowires", *J. of Nanomat.*, 2012, pp. 1-22 (2012).
13. Xu, S. and Wang, Z. "One-dimensional ZnO nanostructures: solution growth and functional properties", *Nano Res.*, **4**(11), pp. 1013-1098 (2011).
14. Soci, C., Zhang, A., Bao, X., Kim, H., Lo, Y., and Wang, D. "Nanowire photodetectors", *J. of Nanosci. and Nanotechnol.*, **10**(3), pp. 1430-1449 (2010).
15. Wang, Z.L. and Song, J. "Piezoelectric nanogenerators based on zinc oxide nanowire arrays", *Sci.*, **312**(5771), pp. 242-246 (2006).
16. Cha, S.N., Seo, J.S., Kim, S.M., Kim, H.J., Park, Y.J., Kim, S.W., and Kim, J.M. "Sound-driven piezoelectric nanowire-based nanogenerators", *Adv. Mater.*, **22**(42), pp. 4726-4730 (2010).
17. Choi, D., Choi, M.Y., Shin, H.J., Yoon, S.M., Seo, J.S., Choi, J.Y., Lee, S.Y., Kim, J.M., and Kim, S.W. "Nanoscale networked single-walled carbon-nanotube electrodes for transparent flexible nanogenerators", *J. Phys. Chem. C.*, **114**(2), pp. 1379-1384 (2010).
18. Hsu, C.L. and Chen, K.C. "Improving piezoelectric nanogenerator comprises ZnO nanowires by bending the flexible PET substrate at low vibration frequency", *J. Phys. Chem. C.*, **116**(16), pp. 9351-9355 (2012).
19. Wang, Z.L. "Piezopotential gated nanowire devices: Piezotronics and piezo-phototronics", *Nano Today*, **5**(6), pp. 540-552 (2010).
20. Wang, Z.L. and Wang, X. "Nanogenerators and piezotronics", *Nano Energy.*, **14**, pp. 1-2 (2015).
21. Liu, J., Fei, P., Song, J., Wang, X., Lao, C., Tummala, R., and Wang, Z.L. "Carrier Density and Schottky Barrier on the Performance of DC Nanogenerator", *Nano Lett.*, **8**(1), pp. 328-332 (2008).
22. Xu, S., Qin, Y., Xu, C., Wei, Y., Yang, R., and Wang, Z.L. "Self-powered nanowire devices", *Nat. Nanotech.*, **5**(5), pp. 366-373 (2010).

23. Zhang, Z., Liao, Q., Yu, Y., Wang, X., and Zhang, Y. "Enhanced photoresponse of ZnO nanorods-based self-powered photodetector by piezotronic interface engineering", *Nano Energy*, **9**, pp. 237-244 (2014).

24. Kumar, R., Singh, R.K., Singh, D.P., Savu, R., and Moshkalev, S.A. "Microwave heating time dependent synthesis of various dimensional graphene oxide supported hierarchical ZnO nanostructures and its photoluminescence studies", *Materials and Design*, **111** (2016).

25. Kumar, R., Singh, R.K., Vaza, A.R., and Moshkaleva, S.A. "Microwave-assisted synthesis and deposition of a thin ZnO layer on microwave-exfoliated graphene: optical and electrochemical evaluations", *RSC. Adv.*, **5**, p. 67988 (2015).

26. Feda, M.H., Khosravi, Y., Darbari, S., and Abdollahi Nejand, B. "Electrically controlled photocatalytic reduction of graphene oxide sheets by ZnO nanostructures, suitable for tunable optoelectronic applications", *IEEE Trans. on Elec. Dev.*, **63**(8), p. 3147 (2016).

27. Darbari, S., Ahmadi, V., Afzali, P., Abdi, Y., and Feda, M. "Reduced graphene oxide/ZnO hybrid structure for high performance photodetection", *J. Nanopart. Res.*, **16**, p. 2798 (2014).

28. Darbari, S., Ahmadi, V., Afzali, P., and Abdi, Y. "Photocatalytic-reduction of GO/ZnO to achieve GNRs for optoelectronic applications", *J. of Phys. D-Appl. Phys.*, **46**, p. 385101 (2013).

29. Ostovari, F., Abdi, Y., Darbari, S., and Ghasemi, F. "Effects of electromechanical resonance on photocatalytic reduction of the free-hanging graphene oxide sheets", *J. Nanopart. Res.*, **15**, p. 1551 (2013).

30. Hummers, W.S. and Offeman, R.E. "Preparation of graphite oxide", *J. Am. Chem. Soc.*, **80**(6), pp. 1339-1339 (1958).

31. Muskens, O.L., Borgstrom, M.T., Bakkers, E.P.A.M., and Rivas, J.G., "Giant optical birefringence in ensembles of semiconductor nanowires", *Appl. Phys. Lett.*, **89**, p. 233117 (2006).

32. Hu, L. and Chen, G. "Analysis of optical absorption in silicon nanowire arrays for photovoltaic applications", *Nano Lett.*, **7**, p. 3249 (2007).

33. Zhang, A., You, S., Soci, C., Liu, Y., Wang, D., and Lo, Y.H. "Photoresponsive properties of ultrathin silicon nanowires", *Appl. Phys. Lett.*, **93**, p. 121110 (2008).

34. Muskens, O.L., Rivas, J.G.M., Algra, R.E., Bakkers, E.P.A.M., and Lagendijk, A. "Design of light scattering in nanowire materials for photovoltaic applications", *Nano Lett.*, **8**, 2638 (2008).

35. Greene, L.E., Law, M., Tan, D.H., Montano, M., Goldberger, J., Somorjai, G. and Yang, P. "General route to vertical ZnO nanowire arrays using textured ZnO seeds", *Nano Lett.*, **5**(7), pp. 1231-1236 (2005).

36. Alver, U., Zhou, W., Belay, A.B., Krueger, R., Davis, K.O., and Hickman, N.S. "Optical and structural properties of ZnO nanorods grown on graphene oxide and reduced graphene oxide film by hydrothermal method", *Appl. Surf. Sci.*, **258**(7), pp. 3109-3114 (2012).

37. Modaresinezhad, E. and Darbari, S. "Realization of a room-temperature/self-powered humidity, sensor, based on ZnO nanosheets", *Sens. and Act. B.*, **237** 358-366 (2016).

38. Dehghan Nayeri, F., Darbari, S., Soleimani, E.A., and Mohajerzadeh, S. "Surface structure and field emission properties of cost effectively synthesized zinc oxide nanowire/multiwalled carbon nanotube heterojunction arrays", *J. Phys. D: Appl. Phys.*, **45**(28), 285101 (2012).

39. Esfandiar, A., Akhavan, O. and Irajizad, A. "Melatonin as a powerful bio-antioxidant for reduction of graphene oxide", *J. Mater. Chem.*, **21**(29), pp. 10907-10914 (2011).

40. Tak, Y., Kim, H., Lee, D., and Yong, K. "Type-II CdS nanoparticle-ZnO nanowire heterostructure arrays fabricated by a solution process: enhanced photocatalytic activity", *Chem. Commun.*, **2008**(38), pp. 4585-4587 (2008).

41. Wang, Y., Wang, F. and He, J. "Controlled fabrication and photocatalytic properties of a three-dimensional ZnO nanowire/reduced graphene oxide/CdS heterostructure on carbon cloth", *Nanoscale.*, **5**(22), pp. 11291-11297 (2013).

42. Zhang, C., Zhang, J., Su, Y., Xu, M., Yang, Z., and Zhang, Y. "ZnO nanowire/reduced graphene oxide nanocomposites for significantly enhanced photocatalytic degradation of Rhodamine 6G", *Physica E.*, **56**, pp. 251-255 (2014).

43. Zhan, D., Ni, Z., Chen, W., Sun, L., Luo, Z., Lai, L., Yu, T., Wee, A.T.S., and Shen, Z., "Electronic structure of graphite oxide and thermally reduced graphite oxide", *Carbon*, **49**, pp. 1362-1366 (2011).

44. Yang, D., Velamakanni, A., Bozoklu, G., Park, S., Stoller, M., Piner, R.D., Stankovich, S., Jung, I., Field, D.A., Ventrice, C.A., and Ruoff, R.S. "Chemical analysis of graphene oxide films after heat and chemical treatments by X-ray photoelectron and micro-Raman spectroscopy", *Carbon*, **47**, pp. 145-152 (2009).

45. Wang, M., Zhou, Y., Zhang, Y., Kim, E.J., Hahn, S.H., and Seong, S.G. "Near-infrared photoluminescence from ZnO", *Appl. Phys. Lett.*, **100**(10), 101906 (2012).

46. He, Y., Zhang, W., Zhang, S., Kang, X., Peng, W. and Xu, Y. "Study of the photoconductive ZnO UV detector based on the electrically floated nanowire array", *Sensors and Actuators A: Physical*, **181**, pp. 6-12 (2012).

47. Bao, J., Shalish, I., Su, Z., Gurwitz, R., Capasso, F., Wang, X., and Ren, Z. "Photoinduced oxygen release and persistent photoconductivity in ZnO nanowires", *Nanoscale Res. Lett.*, **6**(404) (2011).

48. Fu, C., Lee, K.J., Lee, K., and Yang, S.S. "Low-intensity ultraviolet detection using a surface acoustic-wave sensor with a Ag-doped ZnO nanoparticle film", *Smart Mater. Struct.*, **24**(1), 015010 (2015).

49. Zhou, H., Gui, P., Yu, Q., Mei, J., Wang, H., and Fang, G. "Self-powered, visible-blind ultraviolet photodetector based on n-ZnO nanorods/i-MgO/p-GaN structure light-emitting diodes", *J. Mater. Chem. C.*, **3**(5), pp. 990-994 (2015).

50. Chen, H.Y., Liu, K.W., Chen, X., Zhang, Z.Z., Fan, M.M., Jiang, M.M., Xie, X.H., Zhao, H.F., and Shen, D.Z. "Realization of a self-powered ZnO MSM UV photodetector with high responsivity using an asymmetric pair of Au electrodes", *J. Mater. Chem. C.*, **2**(45), pp. 9689-9694 (2014).

51. Roza, L., Fairuzy, K.A.J., Dewanta, P., Umar, A.A., Rahman, M.Y.A., Salleh, M.M. "Effect of molar ratio of zinc nitrate: hexamethylenetetramine on the properties of ZnO thin film nanotubes and nanorods and the performance of dye-sensitized solar cell (DSSC)", *J. Mater. Sci: Mater. Elec.*, **26**, pp. 7955-7966 (2015).

52. Kim, K.H., Kumar, B., Lee, K.Y., Park, H.K., Lee, J.H., Lee, H.H., Jun, H., Lee, D., and Kim, S.W. "Piezoelectric two-dimensional nanosheets/anionic layer heterojunction for efficient direct current power generation", *Sci. Rep.*, **3**(2017) (2013).

Biographies

Lida Shafie received her MSc degrees in 2015 from the Department of Electrical and Computer Engineering, at Tarbiat Modares University (TMU), Tehran, Iran. She has worked on ZnO/rGO-based photodetectors and their application as self-powered sensors, as her master project.

Sara Darbari received her PhD in Electronic Engineering from the University of Tehran, Iran in 2011. She is now an Assistant Professor at ECE Department of Tarbiat Modares University (TMU), Tehran, Iran. Her research interests are electronic, optoelectronic, electromechanic, and energy harvesting devices.

Fatemeh Dehghan Nayeri received her PhD in Nano-Electronics from the University of Tehran, Iran in 2013. Her research interests include nanoelectronics and nanomaterials, solar cells and different kinds of sensors.